Full Paper

Numerical modelling of local scour caused by submerged jets

Sangdo An [1], Hyeyun Ku [2, *] and Pierre Y. Julien [3]

[1] Korea Water Resources Corporation, 200 Sintanjin-ro, Daedeok-gu, Daejeon 306-711, South Korea

[2] Department of Civil Engineering, Seoul National University, 1 Gwanak-ro, Gwanak-gu, Seoul 151-744, South Korea

[3] Department of Civil Engineering, Colorado State University, Fort Collins 80526-1372, Colorado, USA

* Corresponding author, e-mail: hyeyun.ku@gmail.com

Abstract: The local scour downstream of an apron caused by submerged jets issuing from a sluice gate is investigated by means of Flow-3D computational fluid dynamics code. The performance of the numerical model based on renormalisation group $k-\varepsilon$ turbulence scheme and large-eddy simulation (LES) technique is evaluated by comparison with laboratory experiments. Various empirical formulas are coupled with the Flow-3D model to accurately simulate the bedload transport rate. The simulated evolution profiles of local scour are also compared with laboratory experiments. The simulation results show considerable numerical discrepancies between the renormalisation group $k-\varepsilon$ and the LES closure scheme. The Flow-3D model by the LES closure scheme coupled with an appropriate bedload transport formula successfully captures the bed deformation. The simulation results provide a good quantitative means of predicting the formation of both the local scour and the sand dune caused by submerged jets. The present work highlights the potential of the numerical simulation technique and the empirical bedload formulas for the investigation of local scour.

Keywords: computational fluid dynamics, local scour, sediment transport, Flow-3D, environmental engineering

---

INTRODUCTION

Scour in the river environment has received much attention in the engineering field. Hydraulic structures such as dams, sea walls and bridge piers which completely or partially obstruct water flow induce changes in the hydraulic characteristics of the flow. For instance flow acceleration as a result of vertical expansion or contraction in the river causes strong turbulence and channel degradation or aggradation leading to a new equilibrium status [1-2]. In the vicinity of a

hydraulic structure, increase in the transport sediment load may directly result in a local scour. In some cases the scour holes may lead to failure of the hydraulic structure in coastal areas and rivers [3]. Because scouring has been recognised as one of the major causes of collapse of hydraulic structures, prediction of scour development around them is of great importance not only for ensuring their safety, but also for ensuring their effective long-term maintenance.

Many hydraulic structures (e.g. reservoirs and dams) have been constructed and managed in South Korea with the objectives of controlling flood and storing agricultural water. Downstream of a reservoir and dam, bed scour may be formed by plunging jets and submerged jets of periodically released water. To prevent the formation of local scour resulting from jets, currents, waves or eddies, stilling basins and bed protection methods such as horizontal mats or large rock riprap are widely employed. However, in most cases the flow still remains highly turbulent, resulting in local scour of the seabed or streambed downstream of the hydraulic structure. In some cases it may require constructing a bed protection to minimise and move further the scour holes, thus decreasing the risk of a hydraulic structure failure [2]. Figure 1 shows local scour downstream of the concert apron of a low-head dam constructed in South Korea. A multi-beam echo sounder and side-scan sonar system were used to measure the depth and extent of scour holes.
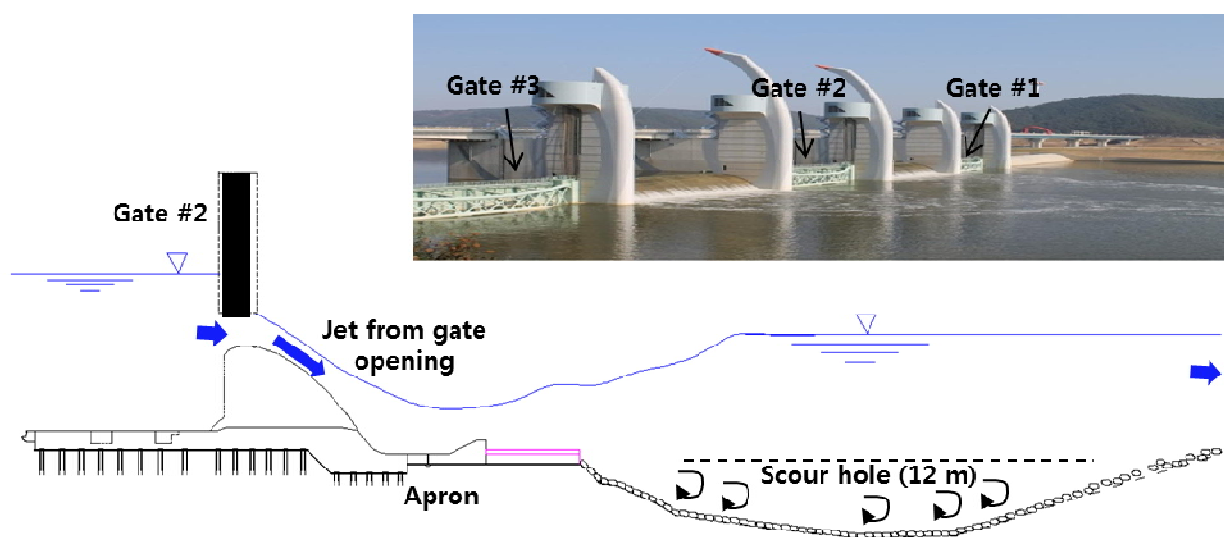

Figure 1. A schematic diagram of local scour downstream of a low-head dam in South Korea based on the bathymetric survey by means of a side-scan sonar system

Many experimental studies have focused on local scour downstream of hydraulic structures such as bed sills in an estuary [4, 5], underflow sluice gates [6] and grade-control structures [7]. Various numerical models for predicting bed changes have been used. One-dimensional sediment transport models have been most often applied to the long-time simulation of reach-scale bed changes [8, 9]. Two-dimensional depth-averaged models, which are widely used in the engineering practice, have been employed so far for local scour modelling [10, 11]. Efforts to simulate local scour with more complicated three-dimensional turbulence closure models have increased since the scouring and sedimentation processes are actually three-dimensional in nature [12, 13]. Direct numerical simulations of the sediment transport forced by steady currents or waves have been performed [14, 15], but they are computationally too intensive and thus generally have not been applied to field-scale applications [16]. In recent years numerical models based on computational

fluid dynamics have been applied to practical sedimentation engineering problems and have shown the good results in predicting the bed deformation in rivers [17-19]. The scour process caused by plunging or submerged jets released from large dams is associated with strong vortexes induced by three-dimensional highly turbulent flows. In this case a three-dimensional numerical model is recommended for the simulation of local scour.

In this study we mainly focus on understanding the local scour process by employing the computational fluid dynamics code, Flow-3D, which is a non-hydrostatic numerical model [20]. We firstly demonstrate the applicability of the code for predicting the shape and depth of a local scour hole by comparing numerical results with those from laboratory experiments reported in the literature [4-7]. An assessment and comparison of turbulence closure schemes using various empirical formulas for bedload sediment transport are then performed. We expect that this study can finally be used to justify the potential of the Flow-3D code after coupling with proper empirical formulas for studying local scour at the field scale.

NUMERICAL MODEL DESCRIPTION

Fluid Flow Model

In this study we employed the Flow-3D code, which is the non-hydrostatic numerical model [20]. The non-hydrostatic numerical simulation constitutes a technological improvement for the movement of sediment particles because hydrostatic models cannot accurately predict the fluid flow and sediment transport in the region where 3-dimensional flows strongly occur [21]. The governing equations solved in Flow-3D are: (1) 3-D Reynolds-averaged Navier-Stokes equations for fluid flow with Boussinesq approximation, (2) the continuity equation and (3) the transport equation for each scalar (e.g. sediment concentration) variable [20]. These equations are given in tensor notations by

$$\frac{\partial u_i}{\partial t} + u_j \frac{\partial u_i}{\partial x_j} = -\frac{1}{\rho_r}\frac{\partial p}{\partial x_i} + \frac{\partial}{\partial x_j}\left(v\frac{\partial u_i}{\partial x_j} - \overline{u_i'u_j'}\right) + g_i\frac{\rho - \rho_r}{\rho_r} \tag{1}$$

$$\frac{\partial u_i}{\partial x_i} = 0 \tag{2}$$

$$\frac{\partial \phi}{\partial t} + \frac{\partial}{\partial x_i}(u_i\phi) = \frac{\partial}{\partial x_i}\left(\Gamma\frac{\partial \phi}{\partial x_i} - \overline{u_i'\phi'}\right) \tag{3}$$

where u_i = mean velocity components in a Cartesian coordinate system (x, y, z), t = time, ρ = density which can be calculated as a function of sediment concentration, ρ_r = reference density, p = total pressure, v = fluid kinematic viscosity, $-\overline{u_i'u_j'}$ = Reynolds stresses, g_i = gravitational acceleration components in each direction, Γ = molecular diffusivity of arbitrary scalar ϕ, and $-\overline{u_i'\phi'}$ = turbulent fluxes of scalar ϕ. The overbar denotes the averaging of fluctuating quantities.

Turbulence Model

The Reynolds stresses ($\overline{u_i'u_j'}$) can be generally modelled using the turbulent viscosity hypothesis [22]:

$$-\overline{u_i'u_j'} = v_t\left(\frac{\partial u_i}{\partial x_j} + \frac{\partial u_j}{\partial x_i}\right) - \frac{2}{3}k\delta_{ij}, \tag{4}$$

where v_t = turbulent (eddy) viscosity, δ_{ij} = Kronecker delta and k = turbulent kinetic energy. In this study we first employed the renormalisation-group (RNG) $k-\varepsilon$ closure scheme [23], in which the eddy viscosity is defined as

$$v_t = c_\mu k^2/\varepsilon , \tag{5}$$

where c_μ = empirical constant and ε = turbulence kinetic energy dissipation rate. In (5) the turbulence kinetic energy (k) and its dissipation rate (ε) are obtained from the following transport equations [20]:

$$\frac{\partial k}{\partial t} + u_j \frac{\partial k}{\partial x_j} = \frac{\partial}{\partial x_j}\left(\frac{v_t}{\sigma_k}\frac{\partial k}{\partial x_j}\right) + P + G - \varepsilon , \tag{6}$$

$$\frac{\partial \varepsilon}{\partial t} + u_j \frac{\partial \varepsilon}{\partial x_j} = \frac{\partial}{\partial x_j}\left(\frac{v_t}{\sigma_\varepsilon}\frac{\partial \varepsilon}{\partial x_j}\right) + c_{1\varepsilon}\frac{\varepsilon}{k}(P + c_{3\varepsilon}G) - c_{2\varepsilon}\frac{\varepsilon^2}{k} , \tag{7}$$

where P and G are defined as

$$P = v_t\left(\frac{\partial u_i}{\partial x_j} + \frac{\partial u_j}{\partial x_i}\right)\frac{\partial u_i}{\partial x_j} , \tag{8}$$

$$G = g_i \frac{v_t}{Sc_t}\frac{1}{\rho_r}\frac{\partial \rho}{\partial x_i} . \tag{9}$$

The parameter values in (5)-(7) obtained from the literature are: c_μ=0.085, $c_{1\varepsilon}$=1.42, $c_{3\varepsilon}$=0.2, σ_k=1.39 and σ_ε=1.39. In the RNG model, $c_{2\varepsilon}$ is a function of the shear rate given [23] by

$$c_{2\varepsilon} = 1.83 + \frac{c_\mu \eta^3(1 - \eta/\eta_o)}{1 + \beta\eta^3} , \tag{10}$$

where $\eta_o = 4.38$, $\beta = 0.015$, $\eta = S k/\varepsilon$ and $S = \sqrt{2S_{ij}S_{ij}}$, S_{ij} representing the strain rate tensor given by

$$S_{ij} = \frac{1}{2}\left(\frac{\partial u_i}{\partial x_j} + \frac{\partial u_j}{\partial x_i}\right) . \tag{11}$$

This study also employed the large-eddy simulation (LES) technique, which provides more detailed information about the interfacial turbulence between bottom and ambient fluids. The LES technique resolves large eddies directly but uses a subgrid-scale turbulence model for small eddies [24].

Sediment Scour Model

Particle dynamics

Most previous studies employed the advection-diffusion relationship (equation 3) to describe the transport of suspended sediment [25-29]. They assumed that particle inertia could be ignored and thus only the mechanism of advection and diffusion affected the transport of suspended sediment. However, some researchers showed that this approach could not fully describe the motion of suspended sediment [30]. In the Flow-3D model a more accurate simulation is obtained by incorporating particle dynamics into the code [16]. The drift velocity of sediment is computed based

on momentum balances for each sediment fraction and fluid-sediment mixture, given in vector forms as:

$$\frac{\partial u_{s,i}}{\partial t} + \overline{u} \cdot \nabla u_{s,i} = -\frac{1}{\rho_{s,i}} \nabla p + F - \frac{K_i}{f_{s,i}\rho_{s,i}} u_{r,i},$$ (12)

$$\frac{\partial \overline{u}}{\partial t} + \overline{u} \cdot \nabla \overline{u} = -\frac{1}{\overline{\rho}} \nabla p + F,$$ (13)

where F is ratio of fluid volume to one computational cell (for example, $F = 1$ indicates that the computational cell is filled with fluid), K_i and $f_{s,i}$ are drag function and volume fraction of sediment respectively, $u_{s,i}$ is velocity of sediment fraction i, $\overline{u}$ and $\overline{\rho}$ are mean velocity and density of fluid-sediment mixture respectively, and $u_{r,i}$ is relative velocity given by

$$u_{r,i} = u_{s,i} - u_f.$$ (14)

The mean density $\overline{\rho}$ is defined as:

$$\overline{\rho} = \sum_{i=1}^{N} f_{s,i}\rho_{s,i} + \left(1 - \sum_{i=1}^{N} f_{s,i}\right)\rho_f$$ (15)

where $\rho_{s,i}$ and ρ_f are densities of sediment fraction i and fluid respectively, and N is number of sediment fractions. Subtracting (13) from (12) gives

$$\frac{\partial u_{drift,i}}{\partial t} + \overline{u} \cdot \nabla u_{drift,i} = \left(\frac{1}{\overline{\rho}} - \frac{1}{\rho_{s,i}}\right)\nabla p - \frac{K_i}{f_{s,i}\rho_{s,i}} u_{r,i}.$$ (16)

The drift velocity $u_{drift,i}$ is defined as:

$$u_{drift,i} = u_{s,i} - \overline{u}.$$ (17)

In (14), $u_{r,i}$ is computed by assuming that the advection term is very small due to the small gradient in drift velocity and the slow motion of sediment in near-steady state at the scale of the computational time:

$$u_{r,i} = \frac{\nabla p}{\overline{\rho} K_i}(\rho_{s,i} - \rho_f)f_{s,i},$$ (18)

where K_i denotes the drag function involving form drag and Stokes drag:

$$K_i = \frac{3}{4}\frac{f_{s,i}}{d_{s,i}}\left(C_{D,i}\|u_{r,i}\| + 24\frac{\mu_f}{\rho_f d_{s,i}}\right),$$ (19)

where $C_{D,i}$ and $d_{s,i}$ indicate drag coefficient and diameter of sediment species respectively, and μ_f is fluid viscosity. The mean flow velocity $\overline{u}$ is determined by computing the velocities of all of the phases:

$$\overline{u} = \left(1 - \sum_{j=1}^{N} f_{s,j}\right)u_f + \sum_{j=1}^{N} f_{s,i}u_{s,j}.$$ (20)

The drift becomes essentially an additional mechanism of sediment transport in the mixture flows with advection and turbulent diffusion.

Entrainment

Entrainment involves the processes of particle pick-up and re-suspension near the bed surface. This needs to be computed in the saltation region (i.e. packed sediment domain). In the model the entrainment of packed sediment is calculated using an empirical model [31]. The entrainment lift velocity of sediment fraction i is the volumetric flux of sediment defined as

$$u_{lift,i} = \alpha_i n_s d_*^{0.3} (\tau_{*,i} - \tau_{*c,i})^{1.5} \sqrt{\frac{\|g\| d_{s,i} (\rho_{s,i} - \rho_f)}{\rho_f}} , \tag{21}$$

where $\tau_{*,i}$ is the local Shields parameter on the bed surface, obtained based on the ratio of hydrodynamic forces to the particle submerged weight, given by

$$\tau_{*,i} = \frac{\tau_o}{\|g\| d_{s,i} (\rho_{s,i} - \rho_f)} . \tag{22}$$

In the Shields parameter, τ_o is the local boundary shear stress and d_* is the dimensionless mean particle diameter defined as

$$d_* = d_{50} \left[\frac{\rho_f (\rho_{s,i} - \rho_f) \|g\|}{\mu_m} \right]^{\frac{1}{3}} , \tag{23}$$

where d_{50} and μ_m are the local mean particle size and the viscosity of a mixture respectively. The critical value of the Shields parameter $\tau_{*c,i}$ corresponds to the beginning of motion of sediment particle. In this model $\tau_{*c,i}$ describes incipient motion on a flat horizontal surface and is computed by the Shields-Rouse equation [32] given by

$$\tau_{*c,i} = \frac{0.1}{R_{*,i}^{2/3}} + 0.054 \left[1 - \exp\left(-\frac{R_{*,i}^{0.52}}{10} \right) \right] \tag{24}$$

where R_* is the Rouse-Reynolds number, defined as

$$R_{*,i} = \frac{\sqrt{0.1(\rho_{s,i} - \rho_f) \rho_f \|g\| d_{s,i}^3}}{\mu_f} . \tag{25}$$

In the case of a sloping bed surface, $\tau_{*c,i}$ should be modified according to the local slope of the bed and the shear force direction. In this study the approach suggested by Soulsby [33], which is similar to the those of Brooks [34] and Julien [35], was employed to account for the effect of the bed slope on sediment transport. The adjusted critical Shields parameter is given by

$$\tau'_{*c,i} = \tau_{*c,i} \frac{\cos\psi \sin\beta + \sqrt{\cos^2\beta \tan^2\varphi_i - \sin^2\psi \sin^2\beta}}{\tan\varphi_i} , \tag{26}$$

where β is the computed angle between the normal to the bed surface and the gravitational acceleration vector g, φ_i is the angle of repose of sediment fraction i, and ψ is the angle between the flow and the upslope direction (Figure 2). If the flow goes up the slope (i.e. $\psi = 0$), (26) then reduces to the formulation of Bormann and Julien [7]:

$$\tau'_{*c,i} = \tau_{*c,i} \frac{\sin(\varphi_i + \beta)}{\sin\varphi_i} . \tag{27}$$

If the flow goes directly down the slope (i.e. $\psi = 180^\circ$), (26) reduces to

$$\tau'_{*c,i} = \tau_{*c,i} \frac{\sin(\varphi_i - \beta)}{\sin \varphi_i}. \tag{28}$$

When the flow is directed laterally across the slope (i.e. $\psi \pm 90^\circ$), (26) becomes identical to the formulation of Lane [36]:

$$\tau'_{*c,i} = \tau_{*c,i} \cos\beta \left(1 - \frac{\tan^2 \beta}{\tan^2 \varphi_i} \right)^{1/2} \tag{29}$$
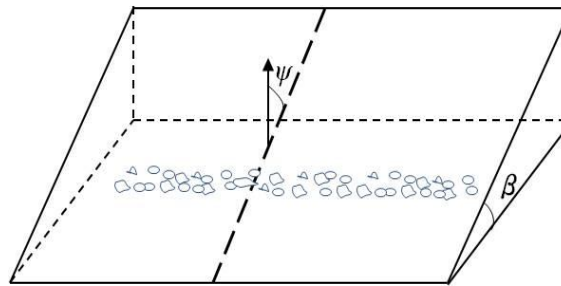

Figure 2. Angles of bedload transport: β is angle between the normal to bed surface and the gravitational vector, and ψ is angle between the flow and the upslope direction.

Bedload transport

Non-cohesive bed particles begin to move when the shear stress on the bed material exceeds the critical shear stress. Generally, finer sediment such as silt and clay is easily entrained and suspended, whereas sand and gravel particles roll and slide in the bed layer or bedload. Most of the bedload transport formulas suggested in the literature were empirically developed. Many of them relate the transport rate to the average shear stress in excess of the critical shear stress. A numerical modelling of small-scale turbulence affecting bedload transport requires an extremely fine mesh size and accurate bed surveys that may be almost impossible to actually perform in field-scale applications. To overcome these problems, an empirical formula may be used to estimate the effects of small-scale turbulence on bedload transport. Table 1 shows the bedload formulas used for this purpose.

Table 1. Bedload transport formulas

Author	Formula
Engelund and Fredsøe [37]	$q_{*,i} = 18.74(\tau_{*,i} - \tau_{*c,i})[\tau_{*,i}^{1/2} - 0.7\tau_{*c,i}^{1/2}]$
Meyer-Peter and Müller [38]	$q_{*,i} = 8(\tau_{*,i} - \tau_{*c,i})^{1.5}$
Nielsen [39]	$q_{*,i} = 12(\tau_{*,i} - \tau_{*c,i})^{1.5}\sqrt{\tau_{*,i}}$

The bedload transport of sediment is quantified by the bedload flux $q_{bv,i}$ that refers to the volume of sediment per unit width per unit time within the bed layer, and is rewritten using the dimensionless bedload flux $q_{*,i}$ [40]:

$$q_{bv,i} = q_{*,i} \sqrt{\left(\frac{\rho_{s,i} - \rho_f}{\rho_f}\right) \|g\| d_{s,i}^3} \, . \tag{30}$$

The Flow-3D model adjusts the time-step size so that the fluid does not flow across more than one cell in one computational time step, δt, which is referred to as a Courant stability criterion [41], defined as:

$$\delta t < 0.45 \cdot \min\left(\frac{V_f \delta x_i}{A_x u}, \frac{V_f \delta y_j}{A_y v}, \frac{V_f \delta z_k}{A_z w}\right), \tag{31}$$

where V_f and A are, respectively, fractional volume and area open to flow in the Favor method [42]. In Flow-3D, if the automatic time-step is selected, the model adjusts the time step to be as large as possible while keeping the stability criteria.

MODEL APPLICATION

Problem Configuration and Simulation Cases

A series of numerical simulations were performed under conditions that corresponded to a laboratory experimental flume set-up for submerged jet scour [6]. This experiment studied the development of a scour hole and sand dune by submerged jets as shown in Figure 3.
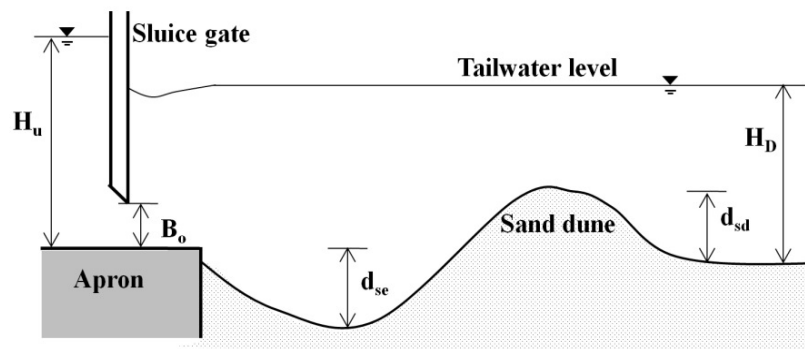

Figure 3. Schematic of scour hole and sand dune development due to turbulent jet

The computational domain was configured in an identical manner with the experimental dimensions (i.e. 406 cm in length, 60 cm in width and 60 cm in height). The erodible bed consisted of 0.4 m of open channel at the end of the rigid apron. The jet flowed out from the sluice gate opening and flowed over the erodible bed consisting of coarse sand (mean particle size (d_{50}) = 0.76 mm, density (ρ_s) = 2,650 kg/m³, porosity (p_o) = 0.43, and angle of repose (φ) =29°). The gate opening (B$_o$) was fixed at 2.0 cm and the jet inlet velocity was 1.56 m/s.

The computational domain for the submerged jet scour simulations with the specified boundary conditions is illustrated in Figure 4. In the laterally-averaged simulation, the computational grid size in the *x*-direction was uniformly set at Δx = 16 mm, whereas the fine grid-spacing ranging between 0.02-0.005 mm was used in the z-direction to increase the simulation speed without significant loss of accuracy. For 3-D simulation, the computational grid was extended in a

lateral (y) direction. Considering the computational constraints, a coarser grid size (Δy = 12 mm) was used in the lateral direction. The domain was comprised of approximately 750,000 cells.
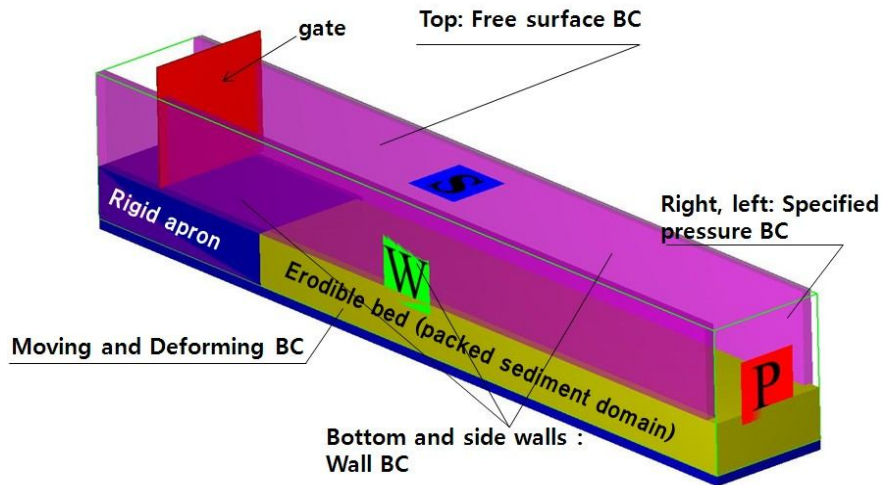

Figure 4. Computational domain depicting erodible region and boundary conditions (BCs) for the simulations corresponding to experiment [6]. W, P and S indicate wall, pressure and symmetry boundary conditions respectively.

The wall boundary is specified as non-tangential stress areas with no-slip condition. At the walls, k and ε were computed using a logarithmic law of wall function [41] given by

$$k = \frac{u_*^2}{\sqrt{c_\mu}}, \varepsilon = \frac{u_*^3}{\kappa \, y_o}, \tag{32}$$

where u_* = shear velocity, κ = von Kármán constant and y_o = the normal distance from the boundary wall to the location of tangential velocity. The packed sediment domain was set as a moving and deforming boundary. It could be deformed only by entrainment or bedload transport. The change in the surface of the packed erodible bed was computed using the current sediment concentration. When the computed sediment concentration in a cell exceeded the packing fraction of the sediment, it meant that all sediment settled down to the bottom and increased the thickness of the packed bed. A volume-of-fluid function was used to track fluid-sediment interfaces [43]. At the free surface no flux conditions were imposed and tangential stresses were zero since all velocity derivatives including velocity components outside the surface were assumed to be zero. The volume-of-fluid function was used to track the location of the free surface in a Eulerian mesh cell. For the inlet and outlet boundaries, the pressure boundary condition with hydrostatic pressure distribution was used to represent the water depth at the downstream end of the erodible bed and upstream end of the flume. The suspended sediment flux and the bedload flux at the inlet were zero since clear water flowed out from the inlet boundary and flowed over the rigid apron without any bedload transport before hitting the sand bed. All conditions for numerical simulations are summarised in Table 2. The numerical simulations were performed on a personal computer with 3.2GHz Quad-core(i7) and 4GB memory. We used the shared-memory parallel version of Flow-3D code allowing for efficient parallelism. We performed the numerical simulations until a steady state was reached, i.e. approximately 10 hours for a 2-D simulation and 1 day for a 3-D simulation.

Table 2. Summary of simulation cases

Case no.	Bed material (sand)				Domain set-up			Numerical option		
	d_{50} (mm)	ρ_s (kg/m^3)	Porosity	p_o	B_o (cm)	H_U (cm)	H_D (cm)	Dimensionality	Turbulence model	Bedload formula
1								2-D	RNG $k-\varepsilon$	Meyer-Peter and Müller [38]
2								2-D	LES	Meyer-Peter and Müller [38]
3	0.76	2650	0.43	29	2.0	41.1	29.1	2-D	LES	Engelund and Fredsøe [37]
4								2-D	LES	Nielsen [39]
5								3-D	LES	Meyer-Peter and Müller [38]

Development of Local Scour

Velocity vectors near the scour hole are shown in Figure 5. They show that the strong submerged jet forms an attached bed-jet on the packed sediment region and induces a recirculating flow region rotating in a counterclockwise direction with flow separation at the top of the sand dune.

In Figure 6 the ratios of U/U_0 are plotted against the corresponding non-dimensional distance x/B_o, where U and U_0 are the depth-maximum horizontal velocity at position x and the inlet jet velocity below the sluice gate respectively. Values of U and U_0 are obtained by the simulations in this study and from experiment investigations in the literature [6].

The jet inlet velocity U_0 was computed to be 1.47 m/s, close to the experimental value of 1.56 m/s. In the rigid apron region the simulation results are very close to the experimental data but show a higher maximum velocity in the far downstream region.
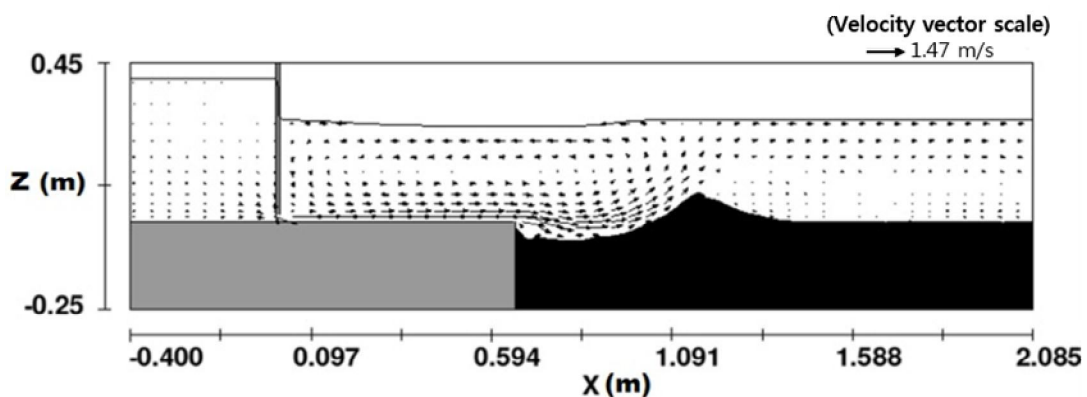

Figure 5. Velocity vectors and scour hole after 3600 sec (Case 5) near equilibrated scour depth of $d_{se} = 0.055$ m
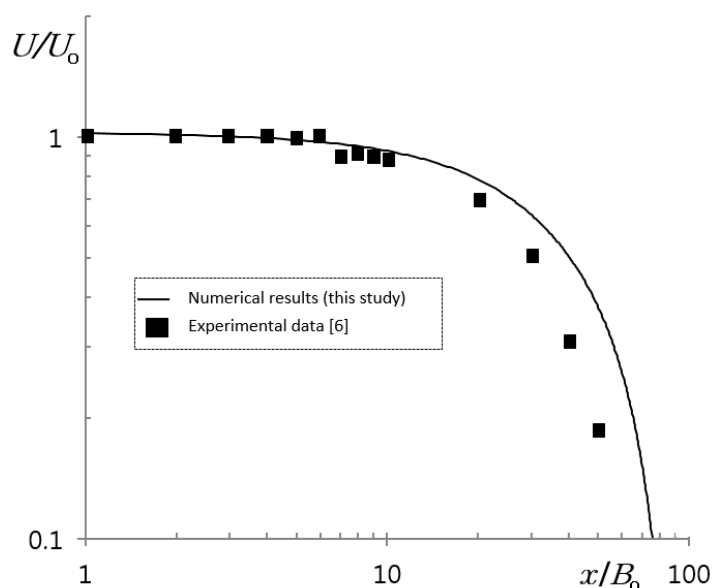
Figure 6. Depth-maximum velocity change along non-dimensional distance x/B_o (x = distance in x-direction and B_o = value of gate opening)

Figure 7 shows the performance of the numerical model using two different turbulence closure schemes, i.e. the RNG $k-\varepsilon$ and the LES schemes, in comparison with the laboratory experiment. Significantly different results were obtained between the two numerical schemes. The limitation of the RNG $k-\varepsilon$ scheme in sediment deposition modelling is that it does not capture the development of any sand dune, resulting in an inaccurate velocity distribution related to the scour process. In comparison, a better description of scour and deposition is achieved using the LES technique, which successfully reproduces the results from the experiment with scour hole formation and sediment deposition. However, the location of the simulated deposition region does not agree well with experimental data: the maximum height of the deposition region, d_{sd} = 0.053 m, and the scour hole, d_{se} = 0.054 m, are underestimated by 23% and 13% respectively.

Applications of various bedload formulas were carried out to improve the predictive capabilities for the development of deposition and the scour and deposition process for this study. Overall, all formulas predicted the scour hole and deposition process rather well. However, the prediction of the aggradation in front of the scour region is still unsatisfactory as shown in Figure 8.

Figure 9 depicts the results of the three-dimensional simulation conducted for comparison with the 2-D modelling. The comparison confirms that the 3-D simulation can improve the accuracy of the reproduction of local scour and deposition processes. In this case the simulation results of case 5 provide a maximum scour depth (d_{se}) of 0.055 m and a deposition height (d_{sd}) of 0.078 m, which agrees well with the measured data from the experiment.
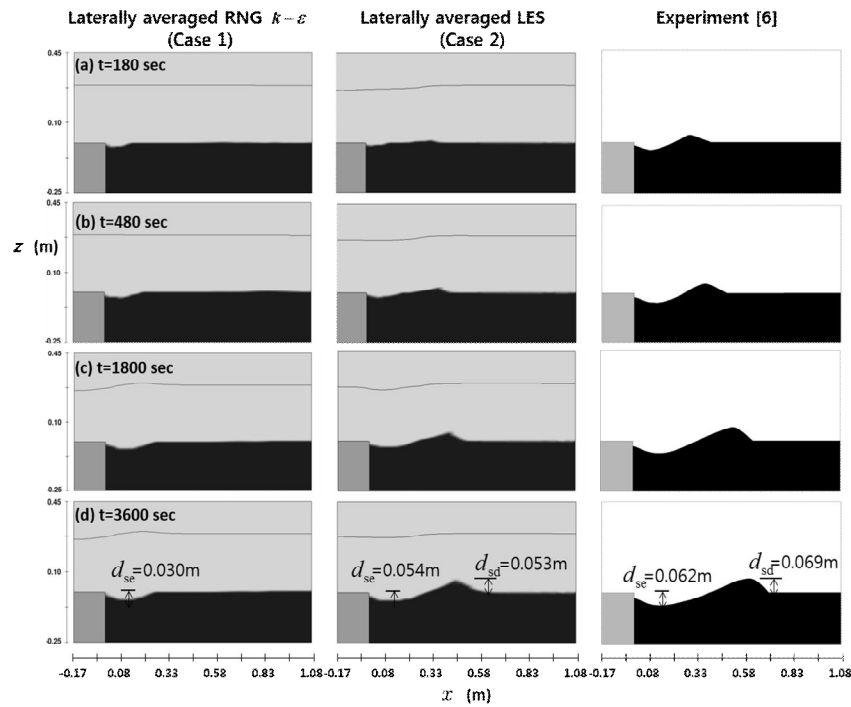
Figure 7. Temporal development of scour hole and sand dune computed using laterally averaged RNG and LES in comparison with experimental results. Computation of bedload transport is based on the Meyer-Peter and Müller formula [38].
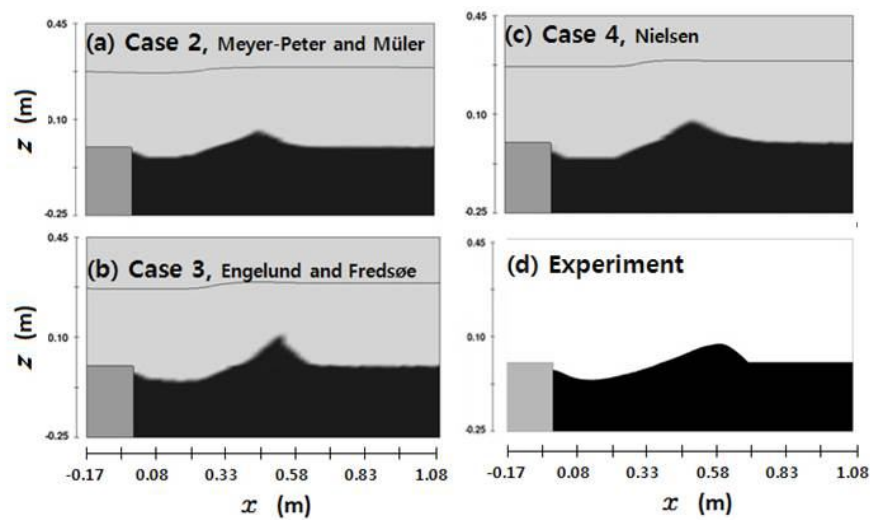

Figure 8. Comparison of bed profiles from tests using different bedload formulas with corresponding experimental data. Numerical results at t = 3600 sec. were used for plotting: (a)-(c) laterally-averaged LES scheme using different bedload formulas; (d) measured data from experiment [6]
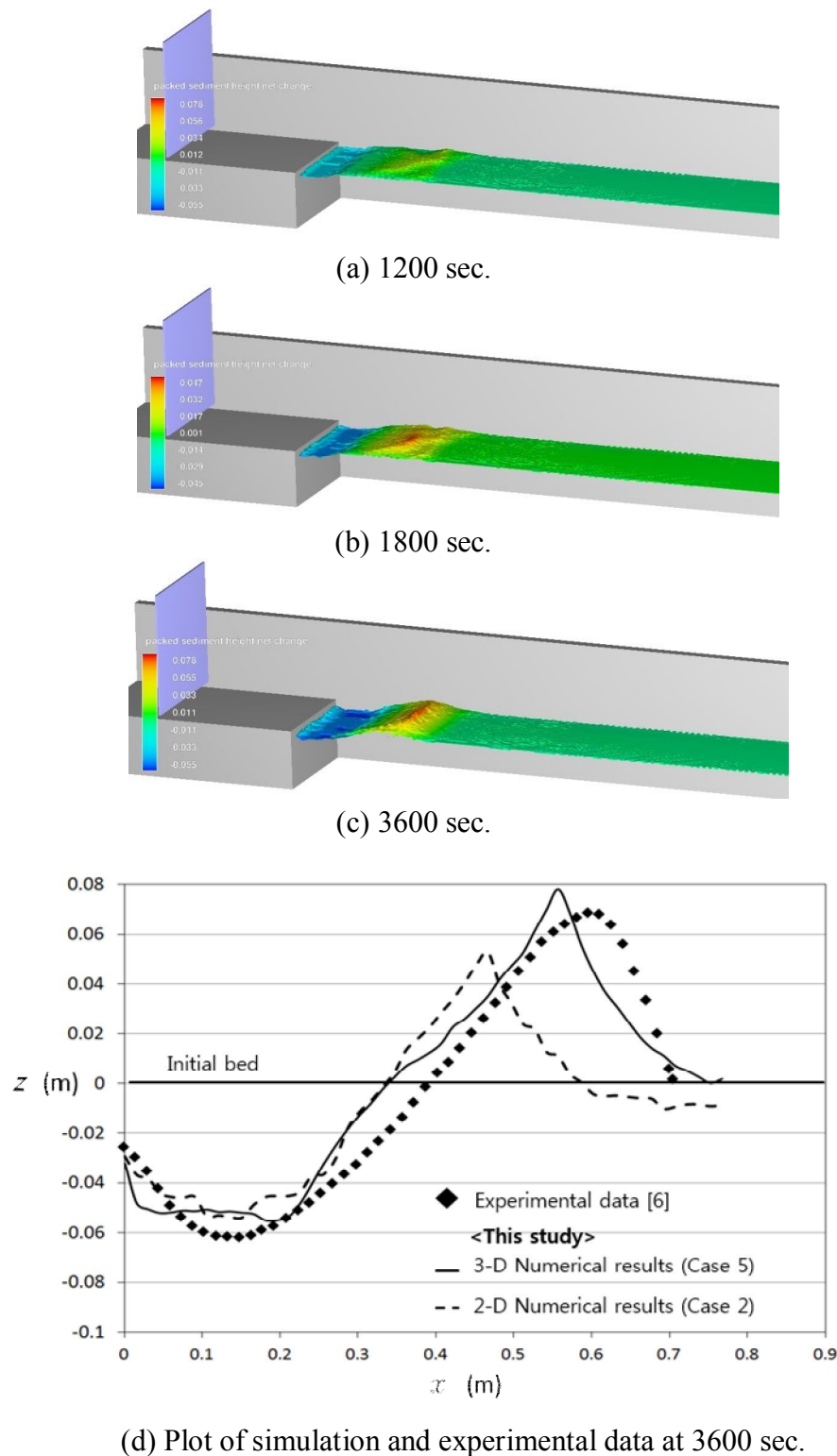
(a) 1200 sec.

(b) 1800 sec.

(c) 3600 sec.

(d) Plot of simulation and experimental data at 3600 sec.

Figure 9. 3-D estimation of bed elevation by LES scheme with Meyer-Peter and Müller formula [38] (case 5) and comparison with case 2 and with experimental data [6]

CONCLUSIONS

Two different turbulence closure schemes, viz. RNG $k-\varepsilon$ and LES have been tested for local scour modelling. The simulation results have shown considerable discrepancies between the two techniques. They clearly demonstrate that the RNG $k-\varepsilon$ closure scheme within the Reynolds-averaged Navier-Stokes framework cannot correctly reproduce the formation of a scour hole and

sand dune. In contrast, a more accurate reproduction of the shapes of both the scour hole and the sand dune is obtainable by employing the LES technique. However, both the direct numerical simulations and the LES schemes are prohibitive for field application because they are computationally very intensive. In this study we have also compared various empirical bedload formulas that can be coupled with the LES scheme, and which can reduce computational time without significant loss in performance. Overall, all formulas are found to predict the depth of the scour hole rather well.

The 2-D simulation accuracy in the prediction of aggradation in front of the scour region is unsatisfactory. A more accurate simulation of sediment transport and bed change is achieved by employing a 3-D model, which successfully captures both the scour hole and the sand dune growth and development.

REFERENCES

1. P. Y. Julien, "River Mechanics", 1st Edn., Cambridge University Press, Cambridge, **2002**, Ch.9.
2. G. J. C. M. Hoffmans and H. J. Verheij, "Scour Manual", CRC Press, Boca Raton, **1997**, Ch. 1.
3. R. Whitehouse, "Scour at Marine Structures: A Manual for Practical Application", Thomas Telford, London, **1998**, Ch. 1.
4. S. Dey and R. V. Raikar, "Scour below a high vertical drop", *J. Hydraul. Eng.*, **2007**, *133*, 564-568.
5. R. Gaudio and A. Marion, "Time evolution of scouring downstream of bed sills", *J. Hydraul. Res.*, **2003**, *41*, 271-284.
6. S. S. Chatterjee and S. N. Ghosh, "Submerged horizontal jet over erodible bed", *J. Hydraul. Div.*, **1980**, *106*, 1765-1782.
7. N. E. Bormann and P. Y. Julien, "Scour downstream of grade-control structures", *J. Hydraul. Eng.*, **1991**, *117*, 579-594.
8. W. Wu, D. Vieira and S. Wang, "One-dimensional numerical model for nonuniform sediment transport under unsteady flows in channel networks", *J. Hydraul. Eng.*, **2004**, *130*, 914-923.
9. R. Ferguson and M. Church, "A critical perspective on 1-D modeling of river processes: Gravel load and aggradation in lower Fraser River", *Water Resour. Res.*, **2009**, *45*, W11424.
10. B. M. Sumer, R. J. S. Whitehouse and A. Tørum, "Scour around coastal structures: A summary of recent research", *Coastal Eng.*, **2001**, *44*, 153-190.
11. W. Wu, R. Marsooli and Z. He, "Depth-averaged two-dimensional model of unsteady flow and sediment transport due to noncohesive embankment break/breaching", *J. Hydraul. Eng.*, **2012**, *138*, 503-516.
12. H. D. Smith and D. L. Foster, "Modeling of flow around a cylinder over a scoured bed", *J. Waterway Port Coast. Ocean Eng.*, **2005**, *131*, 14-24.
13. X. Liu and M. García, "Three-dimensional numerical model with free water surface and mesh deformation for local sediment scour", *J. Waterway Port Coast. Ocean Eng.*, **2008**, *134*, 203-217.
14. K. Bhaganagar and T.-J. Hsu, "Direct numerical simulations of flow over two-dimensional and three-dimensional ripples and implication to sediment transport: Steady flow", *Coast. Eng.*, **2009**, *56*, 320-331.
15. M. W. Schmeeckle and J. M. Nelson, "Direct numerical simulation of bedload transport using a local, dynamic boundary condition", *Sedimentol.*, **2003**, *50*, 279-301.

16. S. An, P. Y. Julien and S. K. Venayagamoorthy, "Numerical simulation of particle-driven gravity currents", *Environ. Fluid Mech.*, **2012**, *12*, 495-513.

17. N. Ruether and N. R. B. Olsen, "Towards the prediction of free-forming meander formation using 3D computational fluid dynamics", Proceedings of Annual Conference on Hydraulic Engineering: Flow Simulation in Hydraulic Engineering, **2006**, Dresden, Germany, pp.31-38.

18. Z. Xie, "Theoretical and numerical research on sediment transport in pressurised flow conditions", *PhD Thesis*, **2011**, University of Nebraska, USA.

19. C. Nitatwichit, Y. Khunatorn and N. Tippayawong, "Computational analysis and visualisation of wind-driven naturally ventilated flows around a school building", *Maejo Int. J. Sci. Technol.*, **2008**, *2*, 240-254.

20. S. D. An, "Interflow dynamics and three-dimensional modeling of turbid density currents in Imha Reservoir, South Korea", *PhD Thesis*, **2011**, Colorado State University, USA.

21. O. B. Fringer, M. Gerritsen and R. L. Street, "An unstructured-grid, finite-volume, nonhydrostatic, parallel coastal ocean simulator", *Ocean Model.*, **2006**, *14*, 139-173.

22. S. B. Pope, "Turbulent Flows", Cambridge University Press, Cambridge, **2000**, pp.359-365.

23. V. Yakhot, S. A. Orszag, S. Thangam, T. B. Gatski and C. G. Speziale, "Development of turbulence models for shear flows by a double expansion technique", *Phys. Fluids*, **1992**, *4*, 1510-1520.

24. W. Rodi, G. Constantinescu and T. Stoesser, "Large-Eddy Simulation in Hydraulics", CRC Press, London, UK, **2013**, Ch.2.

25. A. O. Demuren and W. Rodi, "Calculation of flow and pollutant dispersion in meandering channels", *J. Fluid Mech.*, **1986**, *172*, 63-92.

26. W. A. Thomas, W. H. McAnally and US Army Waterways Experiment Station, "User's Manual for the Generalized Computer Program Systems, Open Channel Flow and Sedimentation, TABS-2: Main Text", Department of the Army, Waterways Experiment Station, Corps of Engineers, Vicksburg (MS), **1985**, Ch.1.

27. L. C. Van Rijn, "Mathematical modeling of suspended sediment in nonuniform flows", *J. Hydraul. Eng.*, **1986**, *112*, 433-455.

28. W. Wu, W. Rodi and T. Wenka, "3D numerical modeling of flow and sediment transport in open channels", *J. Hydraul. Eng.*, **2000**, *126*, 4-15.

29. W. Wu, "CCHE2D-2.1, sediment transport model", Technical report no. NCCHE-TR- 2001-3, National Center for Computational Hydroscience and Engineering, University of Mississippi, **2001**, Ch.1.

30. G. Wang, X. Fu, Y. Huang and G. Huang, "Analysis of suspended sediment transport in open-channel flows: Kinetic-model-based simulation", *J. Hydraul. Eng.*, **2008**, *134*, 328-339.

31. D. R. Mastbergen and J. H. Van Den Berg, "Breaching in fine sands and the generation of sustained turbidity currents in submarine canyons", *Sedimentol.*, **2003**, *50*, 625-637.

32. J. Guo, "Hunter rouse and shields diagram", Proceedings of 13th IAHR-APD Congress, Vol.2, **2002**, Singapore, pp.1096-1098.

33. R. Soulsby, "Dynamics of Marine Sands", Thomas Telford, London, **1997**, pp.107-119.

34. N. H. Brooks, "Mechanics of streams with movable beds of fine sands", *Trans. ASCE,* **1958**, *123*, 525-549.

35. P. Y. Julien, "Erosion and Sedimentation", 2nd Edn., Cambridge University Press, Cambridge, UK, **2010**, Ch.7.

36. E. W. Lane, "Progress report on studies on the design of stable channels by the Bureau of reclamation", *Proc. Am. Soc. Civ. Eng.*, **1953**, *79*, 246-261.

37. F. Engelund and J. Fredsøe, "A sediment transport model for straight alluvial channels", *Nordic Hydrol.*, **1976**, *7*, 293-306.

38. E. Meyer-Peter and R. Muller, "Formulas for bedload transport", Report, 2nd Meeting of International Association of Hydraulic Research, **1948**, Stockholm, Sweden, pp.39- 64.

39. P. Nielsen, "Coastal Bottom Boundary Layers and Sediment Transport", World Scientific, Singapore, **1992**, pp.112-113.

40. J. Brethour and J. Burnham, "Modeling Sediment Erosion and Deposition with the FLOW-3D Sedi-mentation and Scour Model", Flow Science Inc., Santa Fe, **2010**.

41. D. Vanneste, "Experimental and numerical study of wave-induced porous flow in rubble-mound breakwaters", *PhD Thesis*, **2012**, Ghent University, Belgium.

42. C. W. Hirt, "Volume-fraction techniques: Powerful tools for wind engineering", *J. Wind Eng. Ind. Aerodyn.*, **1993**, *46-47*, 327-338.

43. C. W. Hirt and B. D. Nichols, "Volume of fluid (VOF) method for the dynamics of free boundaries", *J. Comput. Phys.*, **1981**, *39*, 201-225.